Preparation and Thermal Characterization of Films Containing Liquid Crystals in a Cellulose Acetate Substrate for Externally Regulated Applications

Alfonso Martínez-Felipe,[1] Enrique Ballester-Sarrias,[1] Corrie T. Imrie,[2] Amparo Ribes-Greus[1]

[1]*Instituto de Tecnología de Materiales, Escuela Técnica Superior de Ingeniería del Diseño, Polytechnic University of Valencia, Camino de Vera S/N, Valencia 46022, Spain*
[2]*Department of Chemistry, University of Aberdeen, Meston Walk, Aberdeen Scotland, United Kingdom*

Received 7 May 2009; accepted 15 August 2009
DOI 10.1002/app.31376
Published online 3 November 2009 in Wiley InterScience (www.interscience.wiley.com).

ABSTRACT: Two different series of polymer dispersed liquid crystal (PDLC) films were prepared for their future use as externally controlled electrolytes in direct methanol fuel cells (DMFC). The liquid crystals used in this work were commercial cholesteryl oleyl carbonate (COC) and *n*-(4-methoxybencylidine)-4-butylanilyne (MBBA); cellulose acetate (CA) was used as the polymer substrate. All the films were characterized by differential scanning calorimetry (DSC) and Thermogravimetric analysis (TGA) to analyze the existence of interactions between the components, the modification of the liquid crystal behavior and the thermal stability of the films. The two series of films exhibited very different behaviors. While the films containing CA and COC maintained most of the properties characteristic of the pure components, including the COC mesomorphism, the analysis of films containing CA and MBBA revealed the existence of strong interactions between the components that promoted the inhibition of the MBBA mesomorphic behavior. © 2009 Wiley Periodicals, Inc. J Appl Polym Sci 115: 3282–3294, 2010

Key words: differential scanning calorimetry (DSC); thermogravimetric analysis (TGA)

INTRODUCTION

During the last years, direct methanol fuel cells (DMFC) have attracted the interest of many researchers and companies because of their advantages with respect to hydrogen fuel cells.[1,2] Since methanol (MeOH) is liquid at room temperature, fuel storage and transport are less complicated than in hydrogen fuel cells. Furthermore, methanol can also be obtained from renewable sources (bio-alcohols). However, DMFC still present several drawbacks, and their technology is not competitive with other fuel cells or energy conversion devices. One of the most important problems of DMFC is the phenomenon known as crossover. Crossover consists on the transfer of unreacted methanol from the anode to the cathode through the electrolyte and occurs when the polymers used in hydrogen fuel cells are applied to DMFC.[1] This phenomenon causes cell efficiency loss of up the 30%, as the MeOH reacts with the oxygen in the cathode in a conventional combustion reaction, and does not contribute to electrical power generation.

Research in DMFC has been focused in the preparation of new polymer electrolytes that suppress crossover of MeOH to the cathode.[1] However, the transport mechanisms of MeOH are strongly related to the proton conductivity through water in the electrolyte, and the morphology of the polymer constitutes a key factor to control the cell performance. Although a great variety of materials has been tested in DMFC, the results are not improving to a great extent those of the commercial materials used in hydrogen fuel cells.[3–5]

In this work we propose the use of polymer dispersed liquid crystals (PDLC) as electrolytes in DMFC. Liquid crystals (LC) are low molecular compounds that exhibit intermediate states between crystalline solids and isotropic liquids. LC can be oriented in the presence of external stimuli such as electrical and magnetic fields[6,7] and therefore can be externally regulated. In PDLCs, LC form a disperse phase in a polymeric substrate, which allows lowering their cost and increasing some of their mechanical properties. Although the polymer is supposed to act as a mere matrix for the liquid crystal aggregates,[8] most of the PDLC show physical and chemical interactions between LC and the polymers. Such interactions can influence the formation of mesophases[9] and also modify the stability of the

Correspondence to: A. Ribes-Greus (aribes@ter.upv.es).
Contract grant sponsor: Spanish Ministry of Science and Innovation; contract grant number: ENE2007-67584-C03-01.

polymeric substrate.[10] Therefore it is important to study the effect of mixing on the resulting morphology before their use, since it can lead to the appearance of interactions and to a change in the individual properties of the components.

In this work we used the solvent evaporation method to prepare two different series of PDLCs films containing cholesteryl oleyl carbonate (COC) and *n*-(4-methoxybencylidine)-4-butylanilyne (MBBA) as the LC and cellulose acetate (CA) as the polymer substrate. Thermal analysis was used to determine the materials properties after their preparation. Differential scanning calorimetry (DSC) was performed on the samples to study the thermal transitions of the components in the mixtures. Thermogravimetric analysis (TGA) was carried out to evaluate the influence of mixing on the thermal decomposition of the components and their stability.

EXPERIMENTAL PROCEDURE

Materials

Two series of films were prepared using the same polymeric substrate with two different commercial LC. CA (powder with $M_r \sim 61{,}000$, 40% acetyl groups, provided by Fluka™) was used as the polymer substrate as it is widely used as a component in membranes for separation purposes.[11,12] On the other hand the LC used in the study were COC (98% purity) and MBBA (98% purity) provided by Sigma-Aldrich™, since both compounds exhibit mesomorphism at low temperatures.[13,14] Acetone was used as the solvent in the preparation of the films.

Films preparation

The solvent evaporation method was used to prepare the films containing 10, 20, 30, 40, 50, 60, and 70% in weight percentage of liquid crystal.[15,16] Initially the CA and the acetone were mixed and stirred during 24 hr to obtain the collodion. Then, the liquid crystal was added to the collodion in the corresponding amounts and stirred again. Finally, the solution containing the liquid crystal, the polymer and the solvent were cast onto a glass plate. The samples were dried slowly at room temperature during several days until constant weight was determined. In both series, macroscopic phase separation was observed in the solutions with contents higher than 70% weight in liquid crystal percentage, thus the corresponding films could not be prepared.

Differential scanning calorimetry (DSC)

The DSC thermograms were performed with a Mettler Toledo DSC 822e (supplied by Mettler Toledo, OH, Columbus) analyser. Around 5 mg of the samples were placed into a sealed aluminum pan, and then heated from −100°C to 150°C (first heating scan). Then the samples were held at 150°C for 3 min and cooled to −100°C (cooling scan). Finally, the samples were held for further 3 min at that temperature again, and then reheated to 150°C (second heating scan). All the scans were performed at a heating rate of 10°C/min under nitrogen atmosphere with a flow rate of 50 mL/min.

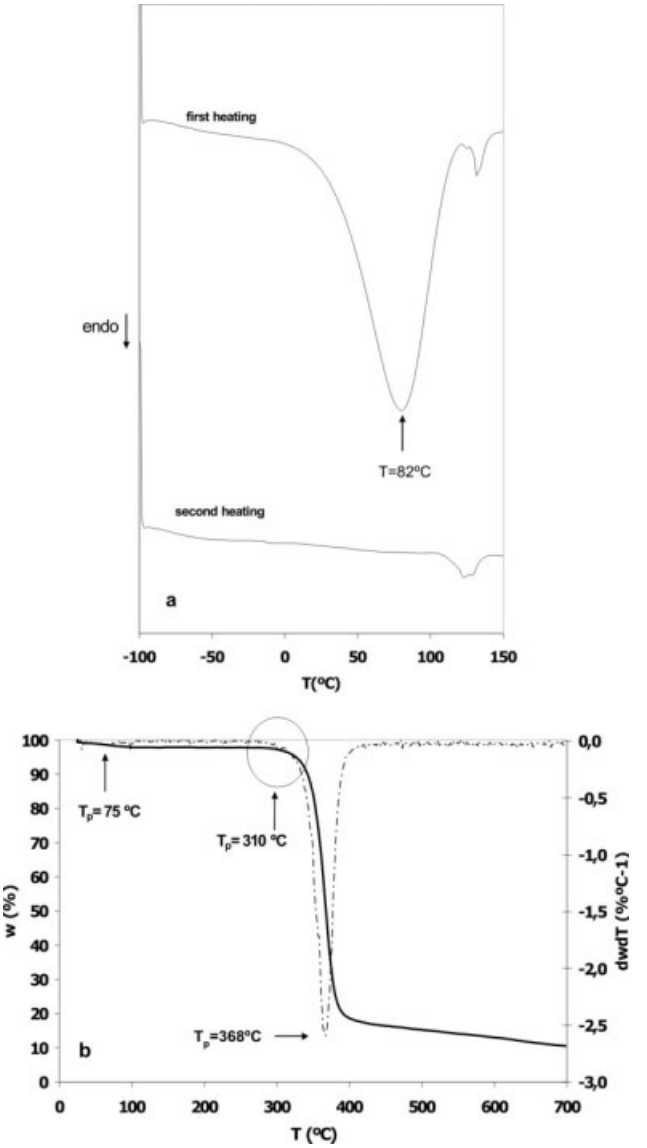

Figure 1 (a) DSC and (b) TG-DTG curves of pure CA.

Thermogravimetric analysis (TGA)

The TGA thermograms were carried out by a Mettler Toledo TGA/SDTA 851 analyser (supplied by Mettler Toledo OH, Columbus). Measurements were performed following a dynamic program from 25 to 700°C at a linear heating rate of 10°C/min under

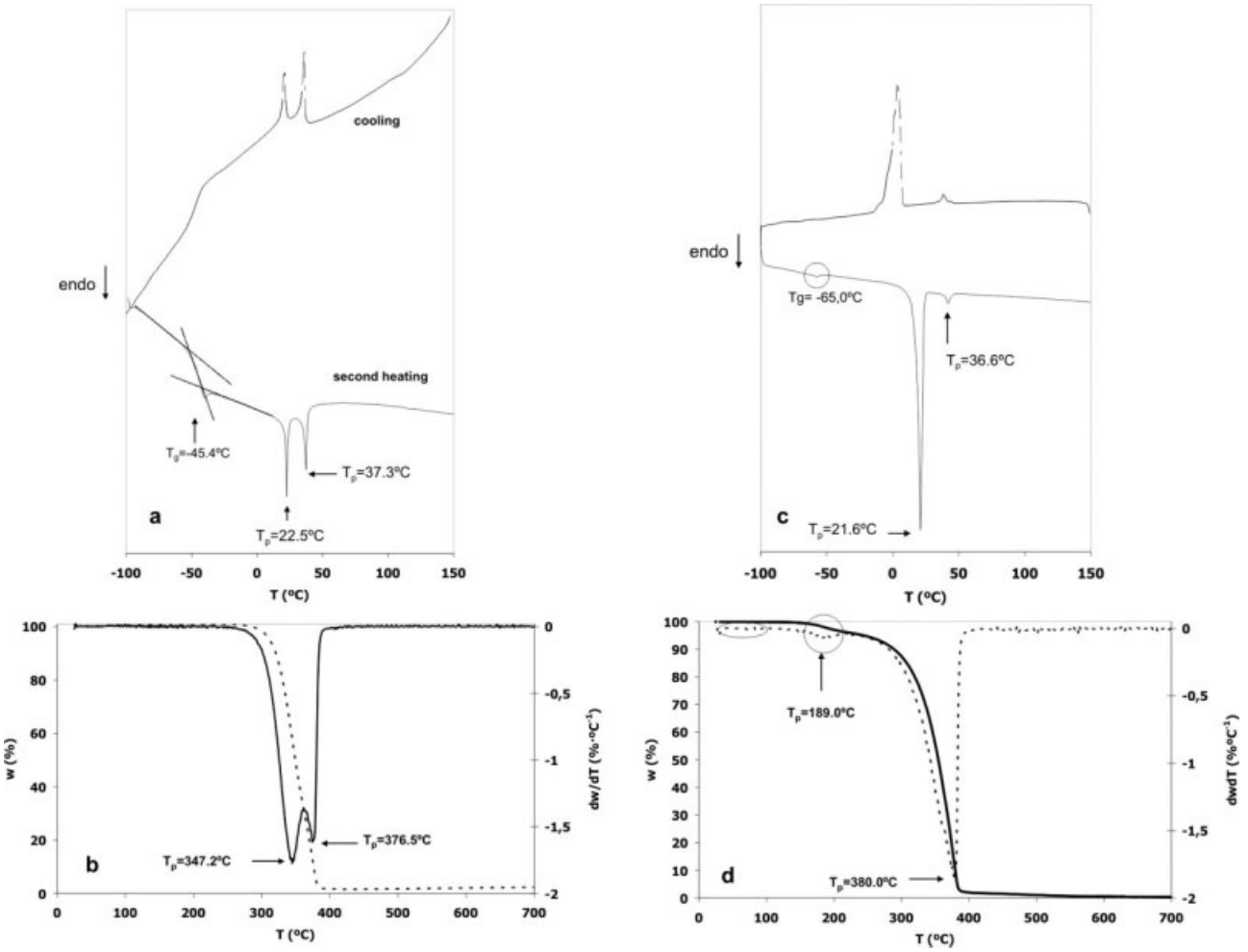

Figure 2 (a) DSC curves of pure COC; (b) TG-DTG curves of pure COC; (c) DSC curves of pure MBBA; (d) TG-DTG curves of pure MBBA.

inert Argon (Ar) atmosphere with a flow rate of 50 mL/min. Sample masses were around 5 mg.

RESULTS AND DISCUSSION

Pure CA

Figure 1(a) shows the DSC thermograms corresponding to the heating scans of the pure CA. The first heating scan shows a broad endothermic process centered at $T = 81.6$°C. The enthalpy associated to this transition was calculated by integration of the DSC curve using a baseline, obtaining a value of $\Delta H = 87.1 \pm 0.1$ J g^{-1}. Since this process does not appear in the second heating scan, other authors associated it to the loss of water initially present in the CA.[17,18] A small endothermic peak is observed in the 130°C region with a very low enthalpy change. Since this peak is visible in the two heating scans with similar enthalpy values, it can be related to a reversible process occurring within the structure of the polymer.

The thermogravimetric (TG) and derivative thermogravimetric (DTG) curves of CA are shown in Figure 1(b). The DTG curve shows a main process centered at $T = 376$°C, corresponding to the pyrolysis of the polymer skeleton backbone, and a secondary process centered at $T = 311$°C that other authors assigned to deacetylation of CA.[18–20] Furthermore, a low weight-loss region appears around 100°C. This peak can be associated to the moisture content in the CA already observed by DSC. The mass loss calculated for this process was $\Delta w = 3.27\%$. The residual fraction of the polymer at 700°C was 10.53%, which is in good agreement with the literature.[18,21,22,23]

Pure COC

The first heating and cooling DSC scans corresponding to the pure COC are shown in Figure 2(a). The glass transition of the liquid crystal is visible at $T_g = -45.4$°C, the smectic to cholesteric transition at $T_{COC\_SC} = 22.5$°C with $\Delta H_{COC\_SC} = 1.29 \pm 0.1$ J g^{-1},

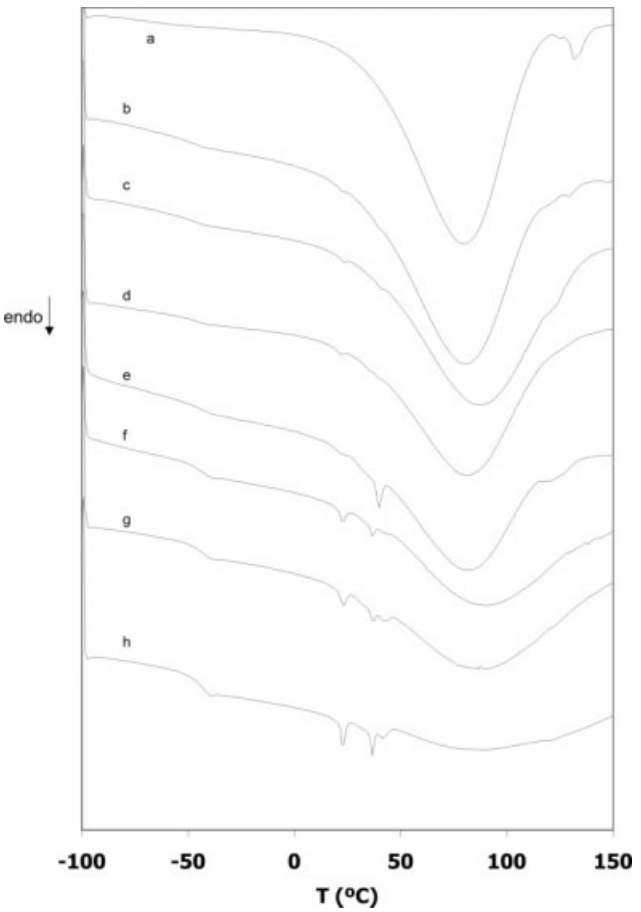

Figure 3 DSC thermograms corresponding to the first heating scan of the samples containing CA and COC: (a) 0, (b) 10, (c) 20, (d) 30, (e) 40, (f) 50, (g) 60, and (h) 70% in weight percentage of COC.

and the cholesteric to isotropic transition at $T_{COC\_CI} = 37.3°C$ with $\Delta H_{COC\_CI} = 1.30 \pm 0.1$ J g^{-1}. The type of mesomorphism was assessed by polarized light microscopy and appraised with literature records.[13]

On the other hand, the TG and DTG curves of COC [Fig. 2(b)] show two processes of decomposition located at $T_{COC\_1} = 345°C$ and $T_{COC\_2} = 376°C$. No significant loss weight in the 100°C region can be observed in the TG curve, which indicates that no moisture or other solvents can be detected in the pure COC sample. The residual fraction of the COC at 700°C was $\Delta w = 2.56\%$.

Pure MBBA

Figure 2(c) displays the DSC thermograms corresponding to the pure MBBA. A small glass transition can be distinguished near $T_g = -65.5°C$. The thermograms also show the phase transitions of the MBBA: the crystalline to nematic transition at $T_{MBBA\_CN} = 21.6°C$ with $\Delta H_{MBBA\_CN} = 46.2 \pm 0.1$ J g^{-1} and the nematic to isotropic transition at $T_{MBBA\_NI} = 36.6°C$ with $\Delta H_{MBBA\_NI} = 1.7 \pm 0.1$ J g^{-1}. The mesomorphism was also assessed by polarized Light Microscopy. The results are in good agreement with the literature.[14]

The TG and DTG curves of MBBA [Fig. 2(d)] show a main asymmetric thermal decomposition process with a maximum at $T_{MBBA\_1} = 380°C$ and a secondary process appearing in the proximity of 189°C (T_{MBBA_2}). A small peak in the 100°C region of the DTG curve indicates the presence of little amounts of solvent in MBBA ($\Delta w = 0.08\%$). The residual fraction of the sample at 700°C was also very low (0.34%).

Films containing CA and COC

Figure 3 shows the DSC thermograms corresponding to the first heating scan of CA, COC, and the CA-COC films containing between 10% and 70% in weight percentage of COC. The thermograms of all the CA-COC films reveal the presence of the endothermic process in the 100°C region, which was previously attributed to the water absorbed in the pure CA. The thermograms also show the process in the

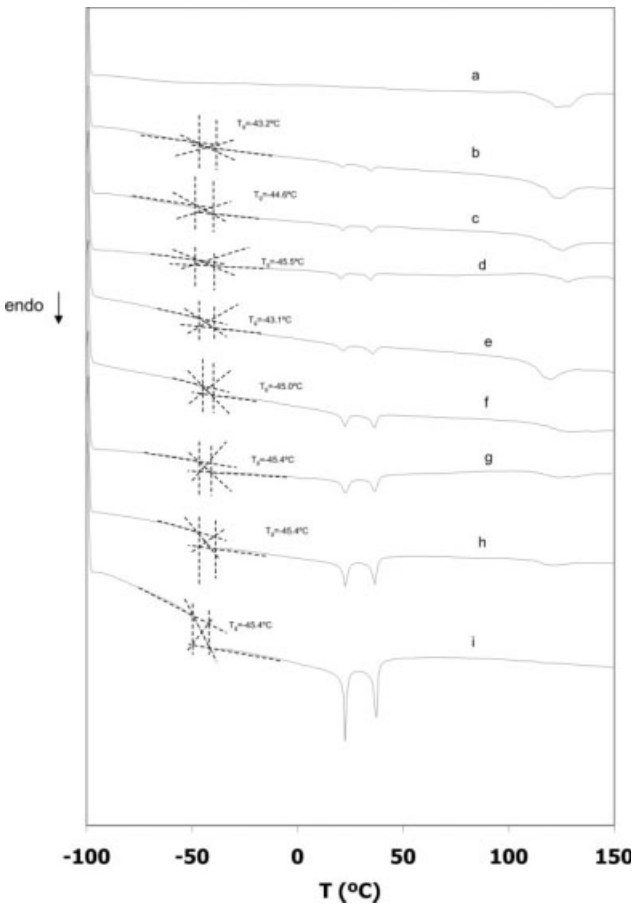

Figure 4 DSC thermograms corresponding to the second heating scan of the samples containing CA and COC: (a) 0%, (b) 10%, (c) 20%, (d) 30%, (e) 40%, (f) 50%, (g) 60%, and (h) 70% in weight percentage of COC.

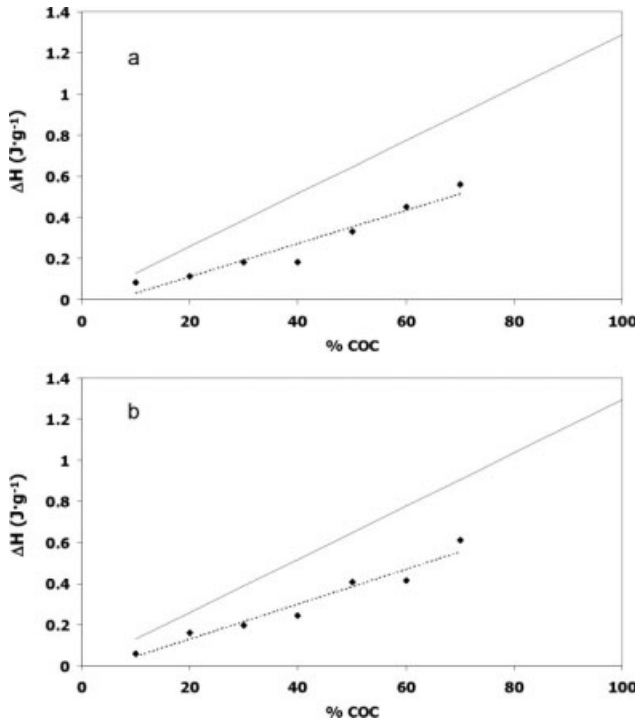

Figure 5 Experimental enthalpies of the COC transitions (◆). The solid lines represent the values considering all the COC contributes to the transition: (a) C→S, (b) S→I transition.

130°C region previously ascribed to CA and discussed above. As expected, the enthalpies corresponding to this process decrease with lower CA percentages in the films, while their T_{max} scarcely changes.

In the same Figure 3 it is also possible to observe two endothermic shoulders at 24°C and 39°C attributed to the COC phase transitions. The study of these transitions in the first heating thermograms can not be carried out as they are overlapped by the endothermic process at 100°C. The glass transition of the liquid crystal is also observed around $T_g = -45$°C in all the composition range. The appearance of all these transitions indicates separation of the components in the films.[24]

Figure 4 shows the curves corresponding to the second heating scan of the films containing CA and COC. The endothermic process related to the water or solvent desorption does not appear, allowing a better observation of the rest of thermal transitions. On the other hand, all the thermograms in Figure 4 show the two phase transitions of COC at $T_{COC\_SC} = 24$°C and $T_{COC\_CI} = 39$°C as well as the glass transition $T_g = -45.4$°C in all the composition range. The appearance of these transitions indicates that the COC maintained its mesomorphic behavior in the films.[17] The mesomorphism of the films was confirmed by polarized light microscopy.

TABLE I
Distribution Coefficient (α), Calculated Using the Enthalpy of the Smectic to Cholesteric (S→C) and Cholesteric to Isotropic (C→I) Transitions in the CA−COC Films

% COC	α (S→C)	α (C→I)
10	0.64	0.46
20	0.43	0.62
30	0.47	0.51
40	0.35	0.47
50	0.51	0.63
60	0.58	0.53
70	0.62	0.67

The enthalpies corresponding to the phase transitions (ΔH_{SC} and ΔH_{CI}) were obtained from the areas of the endothermic peaks in the thermograms in Figure 4. The expected enthalpy values of the transitions ($\Delta H_{exp\_SC} = \Delta H_{COC\_SC} \cdot \frac{\chi}{100}$ for the Smectic to Cholesteric transition SC and $\Delta H_{exp\_CI} = \Delta H_{COC\_CI} \cdot \frac{\chi}{100}$ for the cholesteric to isotropic transition CI) were also calculated based on the enthalpies of the phase transitions observed for the pure COC (ΔH_{COC_SC} and

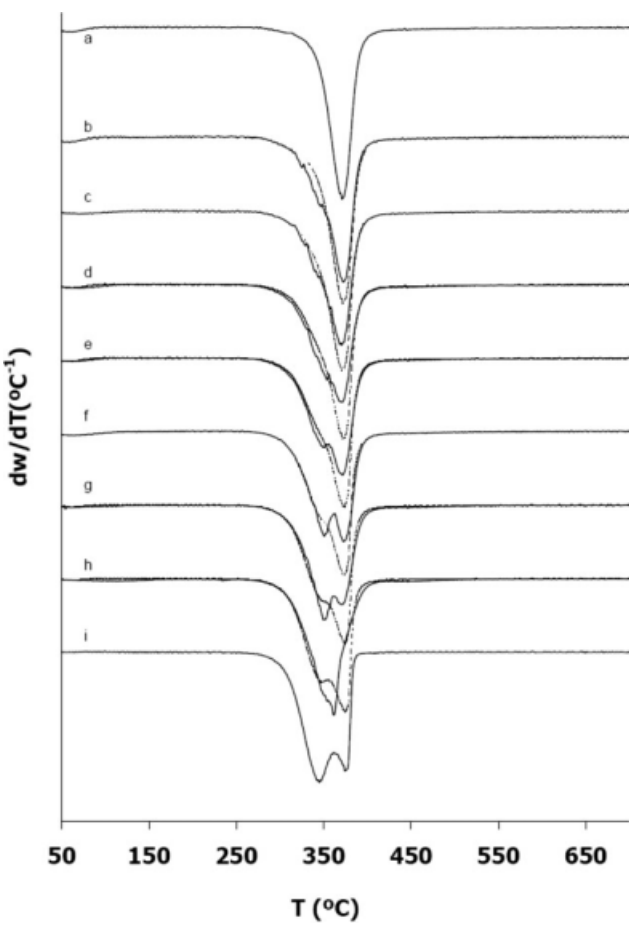

Figure 6 DTG curves of the membranes containing CA and COC: (a) 0, (b) 10, (c) 20, (d) 30, (e) 40, (f) 50, (g) 60, (h) 70, and (i) 100% COC. Dotted lines indicate ideal curves.

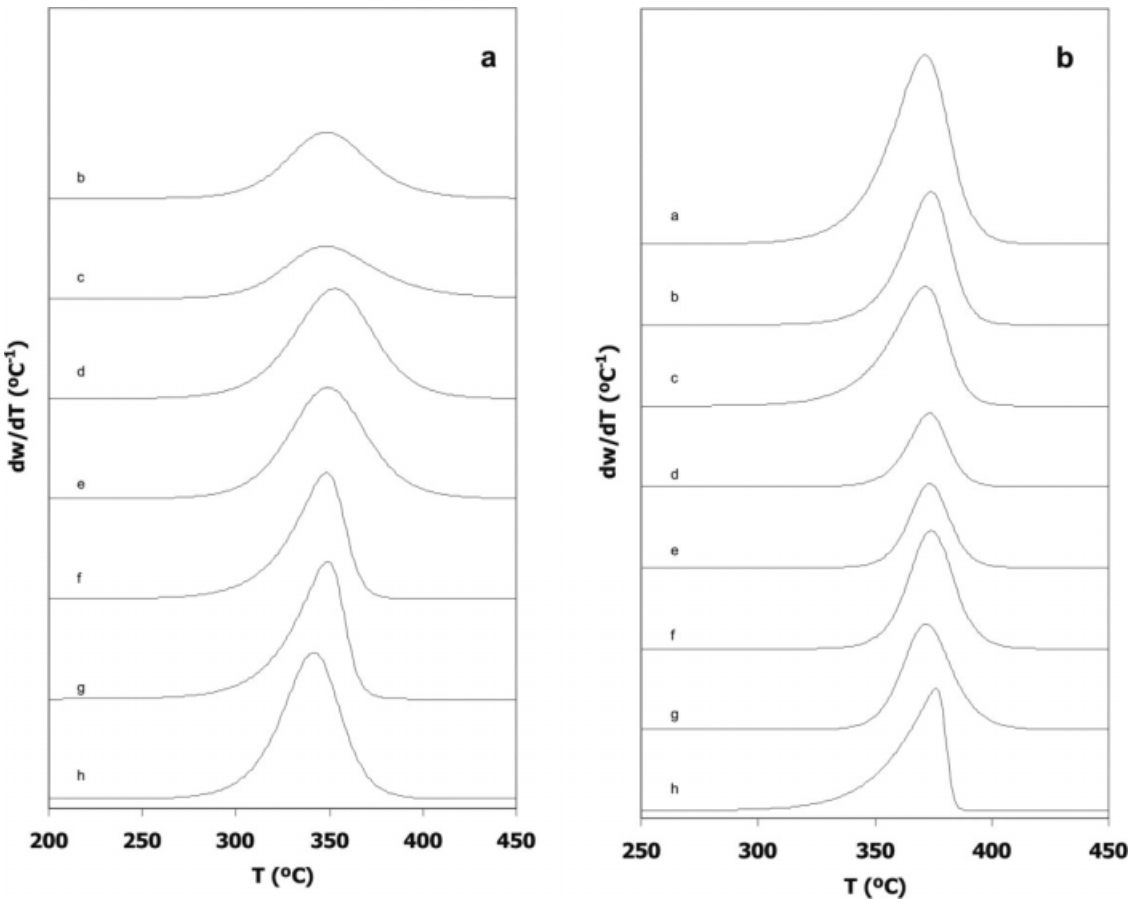

Figure 7 Individual curves corresponding to the deconvolution of the DTG curves of the films containing CA and COC: (a) 0, (b) 10, (c) 20, (d) 30, (e) 40, (f) 50, (g) 60, (h) 100% in COC weight percentage. Figure 7(a) corresponds to the low temperatures peak (peak *b*); and Figure 7(b) to the high temperatures peak (peak *a*).

ΔH_{COC_CI}), where X is the liquid crystal mass percentage in the films ΔH_{exp_SC} and ΔH_{exp_CI} represent the theoretical enthalpy values of the smectic to cholesteric and cholesteric to isotropic transitions in absence of interactions between the components, respectively.

The comparison between the experimental (ΔH_{SC}, ΔH_{CI}) and the expected (ΔH_{exp}) entalphies corresponding to the films containing COC and CA is shown in Figure 5(a,b). As it was expected, ΔH_{SC} and ΔH_{CI} increase at higher COC percentages in the films. However, Figure 5(a,b) evidence differences between the experimental and the expected enthalpies. The deviations between both values in the two transitions indicate that part of the COC does not contribute to the mesomorphism of the films. This behavior was previously reported in other PDLCs and can be attributed to the dissolution of some amount of liquid crystal into the polymer structure.[25,26]

Based on the results of ΔH_{SC}, ΔH_{CI}, and ΔH_{exp}, it is possible to calculate the distribution coefficient

TABLE II
Summary of the Values Corresponding to the Individual Peaks Obtained by Deconvolution of the DTG Curves (CA-COC Films)

	Peak 1/low temperatures				Peak 2/high temperatures			
	Area (%)	T_{peak} (°C)	Width (°C)	Height (°C^{-1})	Area (%)	T_{peak} (°C)	Width (°C)	Height (°C^{-1})
CA					76.94	371.6	28.3	2.331
COC 10%	37.59	348.1	49.2	0.662	44.16	374.0	23.4	1.648
COC 20%	33.43	348.1	55.9	0.524	47.23	371.5	26.7	1.479
COC 30%	61.11	353.0	49.2	1.099	20.52	373.1	20.0	0.908
COC 40%	59.70	349.0	47.6	1.111	23.30	373.2	19.2	1.041
COC 50%	46.04	348.0	30.9	1.259	37.00	374.1	22.6	1.463
COC 60%	48.42	349.2	30.1	1.371	36.06	371.8	24.1	1.308
COC	60.84	341.5	36.6	1.468	38.27	376.5	20.9	1.506

TABLE III
Methods Used in the Kinetic Analysis

Method	Expression	Parameters
Criado[a]	$\frac{z(\alpha)}{z(0.5)} = \frac{f(\alpha)g(\alpha)}{f(0.5)g(0.5)}$ Master curves (theoretical)	$f(\alpha)$
	$\frac{z(\alpha)}{z(0.5)} = \left(\frac{T_\alpha}{T_{0.5}}\right)^2 \cdot \frac{(d\alpha/dt)_\alpha}{(d\alpha/dt)_{0.5}}$ Master curves (experimental)	
Coats-Redfern	$\int_0^\alpha \frac{d\alpha}{f(\alpha)} = \ln\left[\frac{g(\alpha)-g(0)}{T^2}\right] = \ln\left(\frac{k_0 \cdot R}{b \cdot E_{CR}}\right) - \frac{E_{CR}}{R \cdot T}$	E_{CR}
Chang	$\ln\left[\frac{d\alpha/dt}{(1-\alpha)^n}\right] = \ln Z - \frac{E_{Ch}}{R \cdot T}$	n, E_{Ch}
Kissinger	$S = \frac{[d^2\alpha/dt^2]_l}{[d^2\alpha/dt^2]_r}$ $n_K = 1.88 \times S$	n_K

[a] $g(\alpha) = \int_0^\alpha \frac{1}{f(\alpha)} d\alpha$. α is the degree of conversion of the individual process.

$\alpha_i = \Delta H_i / \Delta H_{\exp i}$ for each phase transition i, which represents the COC fraction that remains forming a liquid crystalline phase in the films. The values of α for the two transitions observed in the DSC thermograms are displayed in Table I. The results indicate that there is a considerable amount of COC dissolved into the polymer substrate at any composition, revealing some kind of interactions between the liquid crystal and the polymer even at low COC concentrations.[24] These interactions, however, are not high enough to inhibit the COC mesomorphic behavior in the films.

The thermal stability of the films containing CA and COC was studied by TGA. Figure 6 shows their derivative thermogravimetric curves (DTG).

In the films with low COC concentrations it is possible to distinguish a main degradation process ($T_{max} \sim 370$°C) which can be attributed to the decomposition of CA.[18–20] In the DTG curves it is also possible to observe the appearance of new secondary processes at lower temperatures ($T > 280$°C). Such processes increase with the COC content and therefore can be associated to its presence in the films. At COC weight concentrations of 40% and higher, the degradation of the films seems to occur in at least two main steps (at $T_1 \sim 345$°C and $T_2 \sim 370$°C). The intensities and shapes of the two peaks vary with the COC concentration.

In Figure 6 the ideal DTG curves of the CA and COC films have been also plotted (dotted lines). The ideal curves were built by the adjusted

TABLE IV
Summary of the Results of the Kinetic Analysis (CA-COC Films)

	Coats–Redfern/Criado		Chang		Kissinger
Sample	Model	E_{CR} (KJ mol^{-1})	n_{Ch}	E_{Ch} (KJ mol^{-1})	n_K
	High temperature process				
CA	A3/$n = 1$	272	1.2	313	1.2
COC 10%	$n = 1$	331	1.1	368	1.4
COC 20%	$n = 0.75$	245	0.8	262	1.0
COC 30%	$n = 1.5$	497	1.5	514	1.5
COC 40%	$n = 1.5$	522	1.8	575	1.8
COC 50%	$n = 1.5$	460	1.8	508	1.7
COC 60%	$n = 2$	491	2.1	504	2.0
COC	D2	422	0.25	206	0.4
	Low temperature process				
COC 10%	$n = 2$	216	2	218	2.1
COC 20%	$n = 2$	193	2.4	216	2.5
COC 30%	$n = 1.5$	187	1.7	206	1.7
COC 40%	$n = 1.5$	196	1.8	216	1.9
COC 50%	R3	183	0.7	199	0.9
COC 60%	$n = 0.5$	172	0.5	181	0.8
COC	$n = 1.5$	239	1.5	252	1.5

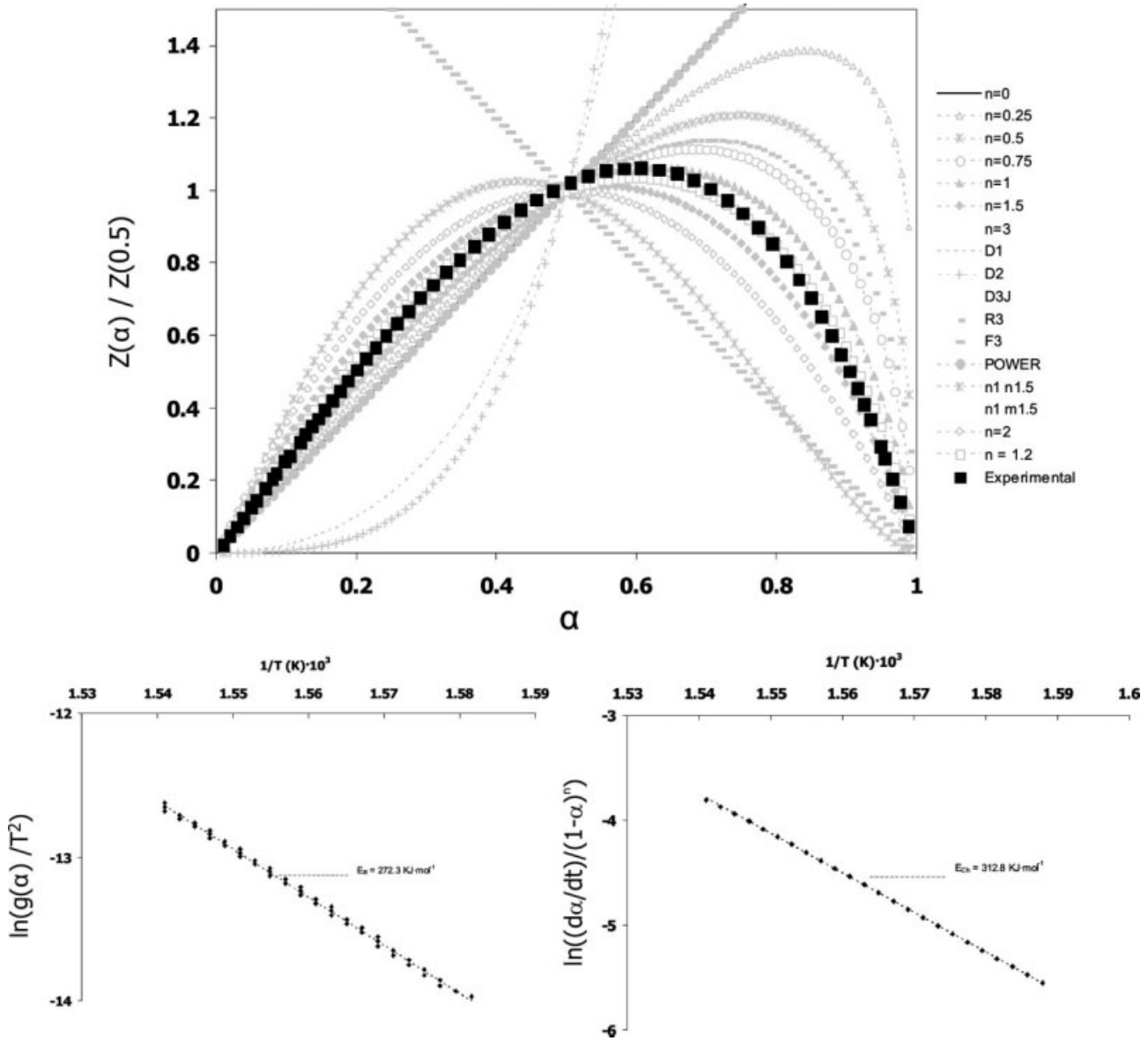

Figure 8 Results of the kinetic analysis applied to the DTG curve of CA: (a) Criado method, (b) Coat-Redfern method, (c) Chang method.

addition of the individual DTG curves of CA and COC at any composition. There are noticeable changes between the experimental and ideal curves shown in Figure 6, suggesting the existence of interactions in the thermal degradation of the CA-COC films.[27] Such interactions are stronger in the films with higher COC contents. This fact suggests the existence of more prominent bulk processes in the degradation of the films with higher COC concentration.[28]

On the other hand, it is worth highlighting that the deviations between the experimental and ideal DTG curves are stronger in the high temperatures range, where the intensity of the DTG experimental curves is lower than expected. It is well-known that the degradation of cellulose and its derivatives can be described as a process of consecutive and competing reactions that can be strongly influenced by the composition.[29,19,20] In this case, the existence of a second phase in the films (evidenced by the DSC results) seems to be responsible for the suppression of some of the decomposition reactions occurring at high temperatures. This fact is coherent with an increase in the residual values at 700°C, which was also observed for all the CA-COC films. All these results suggest that the interactions between CA and COC promote a certain inhibition of the degradation of the polymer substrate.

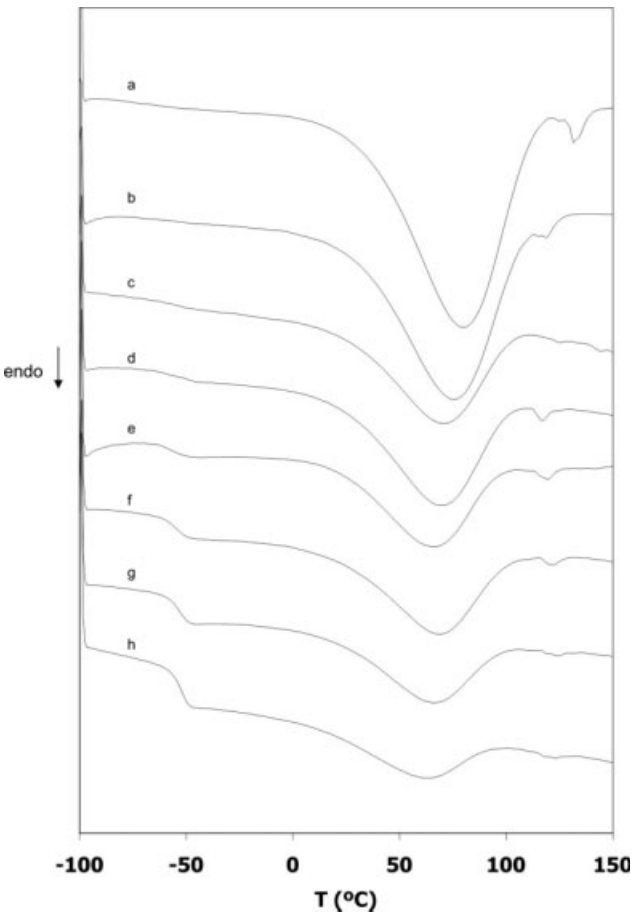

Figure 9 DSC thermograms corresponding to the first heating scan of the samples containing CA and MBBA with: (a) 0, (b) 10, (c) 20, (d) 30, (e) 40, (f) 50, (g) 60, and (h) 70% in weight percentage of MBBA.

As an attempt to perform a more accurate analysis of the thermal degradation of the COC and CA films, the experimental DTG curves were fitted to a sum of asymmetric peaks, according to the following equation:

$$y(x) = y_0 + \sum_{i=1}^{n} A_i \cdot \left(\frac{1}{1 + \exp\left(\frac{-(x - x_{ci} + 0.5)}{w_{2i}} \right)} \right) \times \left(1 - \frac{1}{1 + \exp\left(\frac{-(x - x_{ci} - 0.5)}{w_{3i}} \right)} \right)$$

where y_0 is the baseline of the DTG curve, x_{ci} is a position parameter related to the maximum in the curve, A_i is an amplification parameter and w_{2i} and w_{3i} describe the dispersion and symmetry of the individual curve i. All the DTG curves were satisfactorily fitted to two peaks ($n = 2$) except the curve corresponding to the degradation of pure CA, where only one peak was used.

The individual curves at each composition resulting from the deconvolution are shown in Figure 7(a,b) corresponding to the processes at high (peak *a*) and low (peak *b*) temperatures, respectively. As expected, there are slight changes in the individual curves as a function of the COC content. To quantify such changes, the area, temperature of the maximum (T_{peak}) and width at the maximum intensity were calculated by using the OriginLab software for each individual peak. The results are summarized in Table II.

At low COC concentrations, it is possible to observe a decrease in the values of area of the peak at high temperatures (peak *a*) when the concentration of CA in the films decreases. However, the values of area of the peak at lower temperatures (peak *b*) are too high to be related only to the degradation of COC. This suggests that part of the CA degrades at temperatures lower than expected. On the other hand, the values of T_{peak_b} of the films are higher than those corresponding to the first COC degradation process ($T_{COC\_1} \sim 345$°C). This fact confirms that, in the decomposition of the films, this process

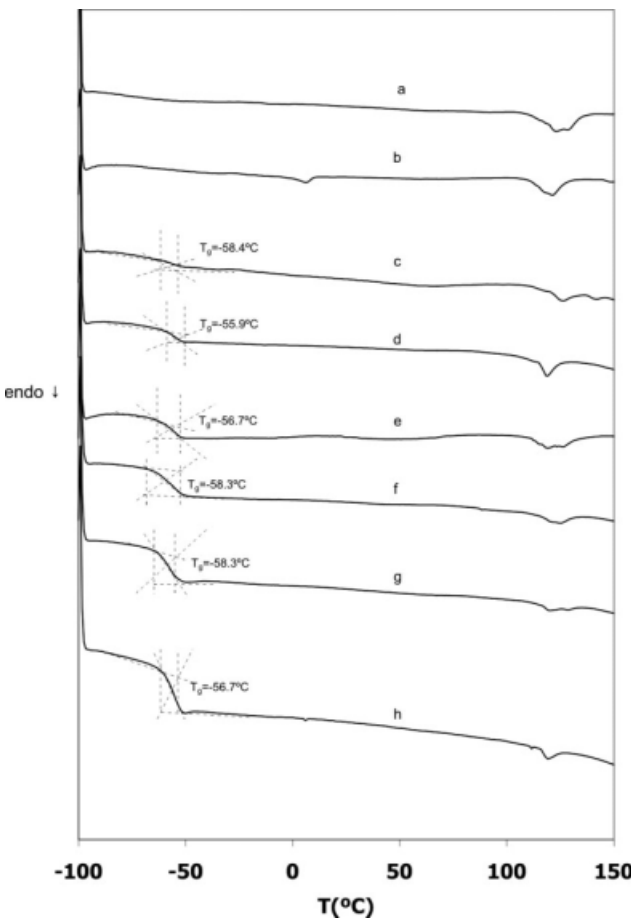

Figure 10 DSC thermograms corresponding to the second heating scan of the samples containing CA and MBBA with: (a) 0, (b) 10, (c) 20, (d) 30, (e) 40, (f) 50, (g) 60, and (h) 70% in weight percentage of MBBA.

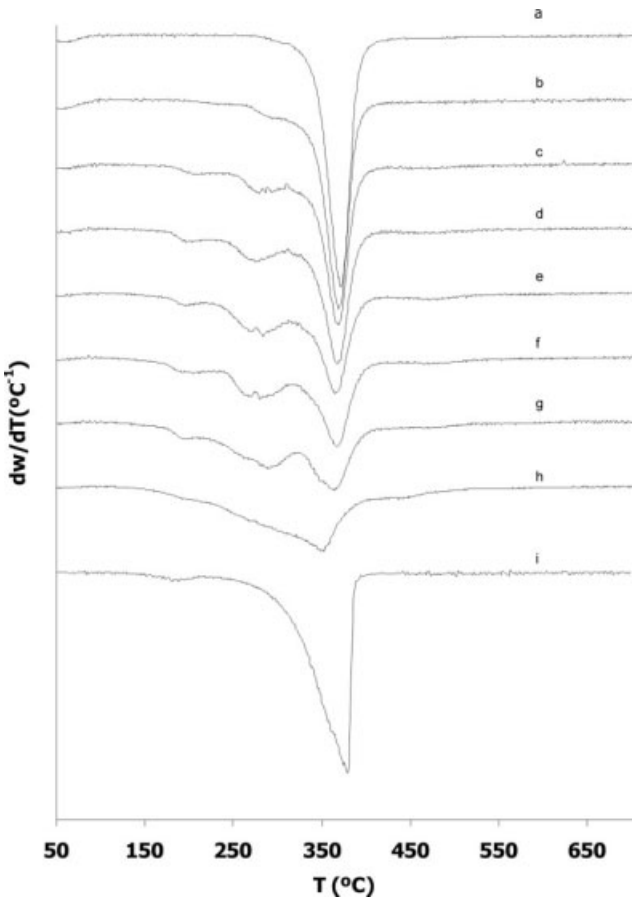

Figure 11 DTG curves of the membranes containing CA and MBBA with: (a) 0, (b) 10, (c) 20, (d) 30, (e) 40, (f) 50, (g) 60, (h) 70, and (i) 100% in weight percentage of MBBA.

may involve the degradation of polymeric chains and not only COC molecules. This result is in agreement with other authors who have previously reported that the existence of low molecular compounds can cause a destabilization of the polymer in PDLCs[29,30]

As it was expected, at high COC concentrations the evolution of the area of peak *b* seems to be more related to the composition of COC in the films. There are not large variations in the temperature range at which this decomposition process occurs. However, it is remarkable that the maximum values of the peak at high temperatures (peak *a*) corresponding to the films appear between those corresponding to the pure components (COC, $T_{COC\_2} \sim 378$°C and CA, $T_{CA} \sim 370$°C). This suggests that the high temperature process may reflect the effect of decomposition of both components

The previous results have shown that the interactions in the thermal degradation of CA and COC promote changes in the shape of the individual decomposition curves, suggesting that the processes of degradation may have changed in the films. To better describe the changes in the thermal degradation of the polymer, the different individual decomposition processes were studied by several methods of kinetic analysis. The Criado method[31] was applied to study the mechanism of decomposition $f(\alpha)$ which best fits to the experimental curves. With that aim, the master curves corresponding to some theoretical models are calculated and compared to those based in the experimental TGA results.

On the other hand, the expression of $f(\alpha)$ of the model which provided the best fit according to the Criado method was used to calculate an apparent activation energy (E_{CR}), by applying the Coats-Redfern method.[32] Additionally, the Chang method,[32] was also applied to estimate the order of the decomposition process, by finding the value of n that provided the best fit of the experimental data and its corresponding activation energy value (E_{Ch}). Finally, the Kissinger method was also used to estimate the values of reaction order (n_K) of the individual processes.[19] The expressions used in the four methods are shown in Table III.

The results of the application of the four kinetic methods to the individual curves obtained by deconvolution are summarized in Table IV. The curves corresponding to the application of the methods to the pure CA are shown in Figure 8.

TABLE V
Summary of Thermogravimetric Results for the Films containing CA and MBBA

	Main process		Low temperature shoulder 1		Low temperature shoulder 2		High temperature shoulder		
	T_{max} (°C)	Weight-loss (%)	T_{max} (°C)	Weight-loss (%)	T_{max} (°C)	Weight-loss (%)	T_{max} (°C)	Weight-loss (%)	Residual (%)
0	370.8	78.35							10.53
10	369.4	63.52	231.4	1.41	303.1	9.55			16.68
20	368.3	52.54	211.2	4.37	287.2	16.51			20.56
30	368.3	48.94	203.8	4.64	277.8	19.03			22.85
40	367.2	39.77	197.4	4.91	279.8	25.96	467.6	2.33	22.75
50	368.6	36.66	199.2	6.94	279.6	26.16	463.7	6.19	22.58
60	363.7	22.03	197.8	6.23	285.6	36.18	405.2	12.40	22.49
70	351.0	7.39	223.2	11.65	319.7	51.48	443.0	8.88	20.82
100	379.6	94.01	188.0	3.37					

According to the Criado method, the curve corresponding to the degradation of pure CA fits very well to an acceleratory process or to a reaction process with values of n slightly higher than $n = 1$ ($n \sim 1.2$) This is in good agreement with the references in which the CA decomposition process is described either as an auto-accelerated process or as a first order process.[21,33,34,35] The values of n calculated by Chang and Kissinger are in good agreement with the Criado method. Despite the slight differences between the activation energies, the values are in good concordance with those reported in the bibliography.[21,33]

However, the reaction order values of peak *a* display values of $n < 1.2$ for the films containing 10 and 20% of COC. Since these processes have been attributed mainly to the degradation of CA, it can be assumed that there is a change in the mechanism of degradation of the polymer in the films, even at low COC concentrations. It is remarkable that the presence of aggregates in the films avoids the random degradation typical in the degradation of long linear polymers.[33,36] The change in the mechanism could also explain the abrupt increase of the residual values. On the other hand, there is a clear increase in the values of n and E_a for this process when the concentration of COC increases in the films. This fact indicates a more complex and energetic degradation mechanism, probably including several species.

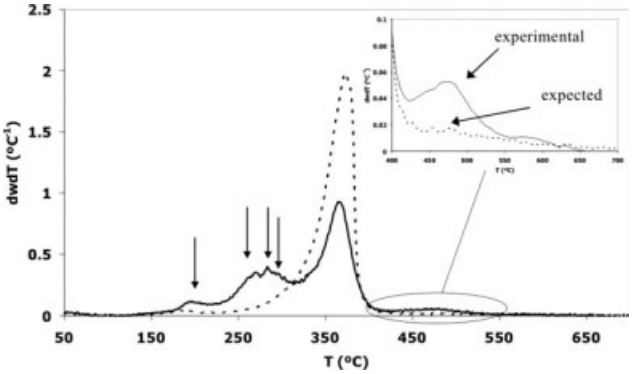

Figure 12 Thermal degradation of the membrane containing 40% of MBBA: (——) experimental and (-----) expected behavior.

Films containing CA and MBBA

The DSC thermograms corresponding to the first heating scan of all the films containing CA and MBBA as well as the pure CA are plotted in Figure 9. All the films containing MBBA exhibit a glass transition in the $T_g \sim -50$°C region in their first heating scans. All the DSC thermograms also show all the peaks related to CA and previously described.

Figure 10 displays the DSC thermograms corresponding to the second heating scans of the films containing CA and MBBA. All the thermograms in Figure 10 show the glass transition in the $T_g \sim -50$°C region. However, the T_g values in the films are slightly higher than that observed for the pure component in Figure 3 ($T_g = -65.0$°C). On the other hand, unlike happened in the DSC thermograms of the COC-CA films, it is not possible to observe the phase transitions associated to MBBA at any composition.[14] This fact suggests that an inhibition of the

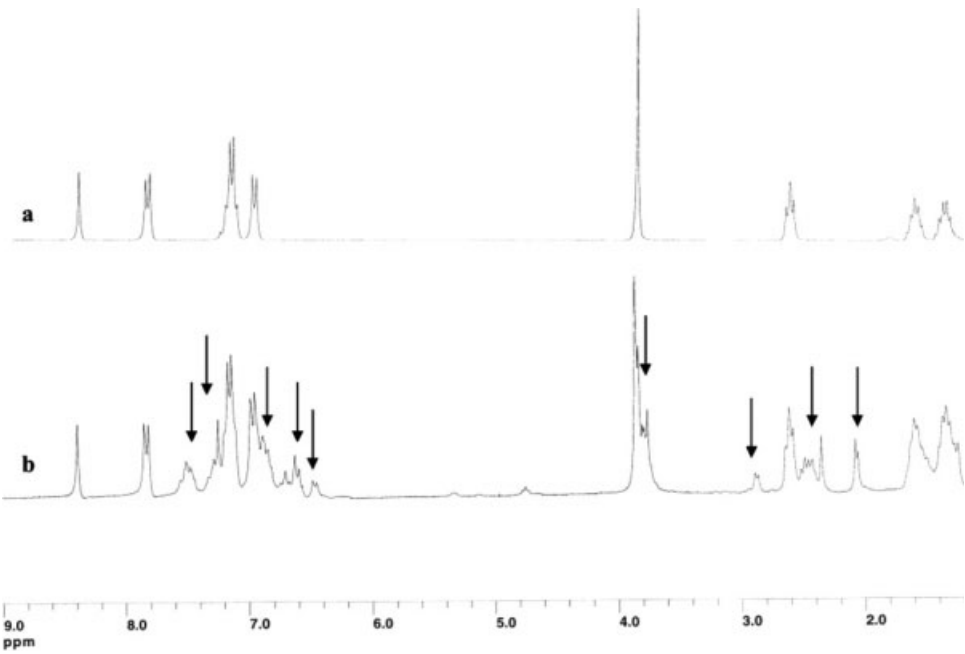

Figure 13 NMR spectra of MBBA: (a) without prior treatment; (b) after extraction from the films.

mesomorphic behavior is taking place in these films.[25,26]

The suppression of some of the MBBA transitions studied by DSC suggests that the MBBA is interacting with the CA in the films even at low temperatures.[9] To study whether these interactions can affect the thermal stability, TGA of the films has been carried out.

The derivative thermogravimetric (DTG) curves corresponding to the films containing MBBA and CA are shown in Figure 11. The curves corresponding to the degradation of CA and MBBA are also displayed. The most representative parameters of the TG and DTG curves were calculated and are summarized in Table V. The main degradation process is observed at $T_{max} = 370°C$ and can be assigned to the decomposition of CA, since it appears at the same temperature region than the pure CA.[18–20] The DTG curves also show the appearance of new peaks at low temperatures (200 and 360°C) as well as at high temperatures (400–500°C).

The ideal DTG curves were built following the same procedure previously used for the COC-CA films. An example can be seen in Figure 12. There are significant differences between the DTG experimental and ideal curves of the CA-MBBA films, indicating the existence of strong interactions in the thermal degradation of the components.[27]

The differences between the curves are especially strong in the 200–360°C region. The appearance of the new processes in this region, where none of the individual components are expected to undergo decomposition processes, suggests that other compounds are present in the films. The fact that the weight-loss corresponding to the new shoulders increases with higher MBBA concentrations in the films suggests that compounds could be derived from the MBBA in the films. Nuclear magnetic resonance (NMR) was performed to a sample of MBBA extracted during the formation process of the films (see Fig. 13). The existence of new signals at 7.5, 7.4, 6.8, 6.6, 6.5, 3.6, 2.9, 2.4, and 2.1 ppm confirmed the existence of new compounds in the sample. The existence of such compounds could be responsible for the inhibition of the MBBA mesomorphic behavior studied by DSC[9]

CONCLUSIONS

Two series of PDLC films showed different behaviors depending on the nature of the liquid crystal and its interactions with the polymer substrate.

The films containing CA and COC maintained their mesomorphic behavior in all the range of compositions, indicating that these films behave as genuine PDLC. However, there was evidence of some interactions between the two components which altered the properties of the polymeric and liquid crystalline phases. Such interactions lead to a decrease in the thermal stability of the first stages of decomposition and also to a certain inhibition of the substrate degradation. The mechanisms of the different decomposition stages vary with the concentration of COC.

On the other hand, the presence of strong interactions was observed in the films containing CA and MBBA even at low temperatures. Such interactions promoted the inhibition of the mesomorphic properties of MBBA in these films. This fact was also accompanied by a decrease in the thermal stability of the samples.

Therefore, the membranes containing CA and COC are candidates for their use in electrolytic applications, since they maintain the mesomorphic properties and do not suffer a drastic decrease in their thermal stability, while the films containing CA and MBBA had poor chemical and thermal stability, which lead to a suppression of the liquid crystallinity.

References

1. Blomen, L. J.; Mugerwa, M. N., Eds. Fuel Cell Systems, Plenum Press: New York, 1993.
2. Dyer, C. K. J Power Sources 2002, 106, 31.
3. Kim, D. S.; Parka, H. B.; Rhim, J. W.; Lee, Y. M. Solid State Ionics 2005, 176, 117.
4. Shin, J. P.; Chang, B. J.; Kim, J. H.; Lee, S. B.; Suh, D. H. J Membr Sci 2005, 251, 247.
5. Schauer, J.; Kůdela, V.; Richau, K.; Mohr, R. Desalination 2006, 198, 256.
6. Collings, P. J.; Hird, M., Eds. Introduction to Liquid Crystals. Chemistry and Physics, Taylor & Francis: New York, 1997.
7. Demus, D.; Goodby, J.; Gray, G. W.; Spiess, H. W.; Vill, V., Eds. Handbook of Liquid Crystals. Fundamentals, Wiley-VCH: New York, 1998.
8. Mucha, M. Prog Polym Sci 2003, 28, 837.
9. Crawford, G. P.; Zumer, S., Eds. Liquid Crystals In Complex Geometries Formed by Polymer and Porous Networks, Taylor and Francis: New York, 1996.
10. Filip, D.; Simionescu, C. I.; Macocinschi, D. Polym Degrad Stab 2001, 72, 377.
11. Smitha, B.; Suhanya, D.; Sridhar, S.; Ramakrishna, M. J Membr Sci 2004, 241, 1.
12. Edgar, K. J.; Buchanan, C. M.; Debenham, J. S.; Rundquist, P. A.; Seiler, B. D.; Shelton, M. C.; Tindall, D. Prog Polym Sci 2001, 26, 1605.
13. Lin, Y. Y.; Chen, K. S.; Lin, S. Y. J Controlled Release 1996, 41, 163.
14. Sorai, M.; Nakamura, T.; Seki, S. Pramana Suppl 1975, 1, 503.
15. Kajiyama, T.; Nagata, Y.; Washizu, S.; Takayanagi, M. J Membr Sci 1982, 11, 39.
16. Kajiyama, T.; Kikuchi, H.; Shinkai, S. J Membr Sci 1988, 36, 243.
17. Shieh, J. J.; Chung, T. S. J Membr Sci 1998, 140, 67.
18. Arthanareeswaran, G.; Thanikaivelan, P.; Srinivasn, K.; Mohan, D.; Rajendran, M. Eur Polym J 2004, 40, 2153.
19. Huang, M. R.; Li, X. G. J Appl Polym Sci 1998, 68, 293.
20. Chatterjee, P. K.; Conrad, C. M. J Polym Sci, Part A: Polym Chem 1968, 6, 3217.
21. Lucena, M. C.; Alencar, A. V.; Mazzeto, S. E.; Soares, S. A. Polym Degrad Stab 2003, 80, 149.

22. Alvarez, V. A.; Vázquez, A. Polym Degrad Stab 2004, 84, 13.
23. Rao, R. V.; Ashokan, P. V.; Shridhar, M. H. Polym Degrad Stab 2000, 70, 11.
24. Filip, D.; Simionescu, C. I.; Macocinschi, D.; Paraschiv, I. J Therm Anal Calorim 2001, 65, 821.
25. Smith, G. W. Mol Cryst Liq Cryst 1990, 180, 201.
26. Smith, G. W.; Ventouris, G. M.; West, J. L. Mol Cryst Liq Cryst 1992, 213, 11.
27. Turi, E. Thermal Characterization of Polymeric Materials, Academic Press: New York, 1997; Vol 2, p 864.
28. Zhou, Y. W.; Jaroniec, M.; Gilpin, R. K. J Colloid Interface Sci 1997, 185, 39.
29. Yang, P.; Kokot, S. J Appl Polym Sci 1996, 60, 1137.
30. Filip, D.; Simionescu, C. I.; Macocinschi, D. Thermochim Acta 2003, 395, 217.
31. Criado, J. M. Thermochim Acta 1978, 24, 186.
32. Chang, W. L. J Appl Polym Sci 1994, 53, 1759.
33. Capart, R.; Khezami, L.; Burnham, A. K. Thermochim Acta 2004, 417, 79.
34. Varhegyi, G.; Antal, M. J.; Szekely, T.; Piroska Szabo, P. Energy Fuels 1989, 3, 329.
35. Prout, E. G.; Tompkins, F. C. Trans Faraday 1944, 40, 488.
36. Wall, L. A.; Madorsky, S. L.; Brown, D. W.; Straus, S.; Simha;, R. J Am Chem Soc 1954, 76, 3430.